JTTEE5 11:244-252

Peer Reviewed

Volatilization of Metal Powders in Plasma Sprays

A. Vardelle, M. Vardelle, H. Zhang, N.J. Themelis, and K. Gross

(Submitted 6 February 1999; in revised form 1 March 2000)

Ideally, plasma spraying of metal powders must take place within a narrow processing "window" where the particles become fully molten before they hit the substrate, but are not overheated to the point that substantial volatilization occurs. Metal evaporation in flight results in a decrease in the deposition efficiency. In addiiton, the emission of vapors leads to the formation of metal and oxide fumes that are undesirable from the viewpoints of both resource conservation and environmental control. This study examines the vaporization and fume formation in the plasma spraying of iron powders of different size ranges. The experimental part involves the determination of the population (number density) of metal atoms at different cross sections along the trajectory of the plasma jet, and the collection of the submicronic particles resulting from vapor condensation. The experimental results are compared with the projections of a mathematical model that computes the gas/particle velocity and temperature fields within the jet envelope, projects the rate of heat/mass transfer at the surface of individual particles, and determines the rate of volatilization that results in the formation of metal and metal oxide fumes.

Keywords absorption spectroscopy, metal fumes, modeling, plasma spraying of metals, powder volatilization

1. Introduction

The basic steps involved in any thermal spray process are substrate preparation, masking and fixturing, coating finishing, inspection, and stripping as necessary. Substrate preparation usually involves scale and oil/grease removal, as well as surface roughening. Roughening is necessary in most applications to ensure adequate bonding of the coating to the substrate. During the spray process, environmental concerns, both from resource conservation and pollution prevention points of view, include the generation of dust, fumes, excess overspray beyond the part to be coated, and particles that have not penetrated into the jet at the injection point. Emissions are contained in an exhaust hood and the gas handling system consists of either a filter bag system or a "water curtain" and a wet scrubber. In the latter case, a wet sludge is obtained and the scrubber water is recirculated. In general, residues from the thermal spraying process include dust and fume by-products, spent exhaust filters, rejected parts, and waste associated with the grinding and finishing phases.[1]

For metallic coatings, the deposition efficiency and the amounts of fume and dust by-products depend principally on the powder injection efficiency in the plasma jet, and the oxidation/volatilization phenomena within the plasma jet cone. These phenomena affect both resource utilization (i.e., the use of metal powder) and pollution prevention (i.e., minimization of dust and fume by-products).

The objective of this study was to investigate the vaporization of metal powders under plasma conditions. The density (concentration) of metal atoms in different cross sections of the plasma jet was measured by absorption spectroscopy. The size range of the dust resulting from vapor condensation was determined by means of an electrical low-pressure impactor to be described later. The study included a two-dimensional (2D) simulation of the spray process that predicts the degree of particle vaporization.

2. Experimental Procedure

2.1 Plasma Spraying

Plasma spraying in air was performed using a custom-built plasma gun. Commercial iron powders were used with particle size distributions of 14-55, 45-90, 80-100, and 125-160 μm. Powders were injected through a 1.8 mm diameter port located 3 mm downstream of the nozzle exit and 6.5 mm from the gun axis. The flow rate of the carrier gas (argon) was fixed so that the median trajectory of the spray jet was at an angle of 3-5° to the plasma jet centerline.

Two sets of spraying parameters were used. In the first one, the total gas flow rate was fixed at 60 slm and the hydrogen content of the plasma-forming gas was varied between 0% and 25% (Table 1). The specific enthalpy input to the gas was set to 5.8 MJ/kg irrespective of the hydrogen content, i.e., the arc current was increased so as to compensate for the voltage decrease at low hydrogen content. In the second set of spraying parameters, the hydrogen content of the plasma gas was fixed at 25% and the arc current was varied from 300-600 A (Table 2).

This paper was presented at the International Thermal Spray Conference sponsored by the ASM Thermal Spray Society, the DVS–German Welding Society and the IIW International Institute of Welding, May 8–11, 2000 in Montreal, Canada.

A. Vardelle and **M. Vardelle,** University of Limoges, Laboratory, Sciences des Procédés Céramiques et de Traitements de Surface, 87060 Limoges, France; **H. Zhang** and **N.J. Themelis,** Earth and Environmental Engineering, Columbia University, New York, New York 10027; and **K. Gross,** School of Materials Engineering, Monash University, Victoria 3800, Australia. Contact e-mail: armelle@ensil.unilim.fr.

Nomenclature

a	thermal accommodation coefficient
A_{ul}	transition probability from level u to level l
B	Spalding number
c	concentration
C_D	dimensionless drag coefficient
C_p	specific heat at constant pressure
C_ν	shape factor taking into consideration line broadening by Doppler and Lorentz effects
D_{AB}	diffusivity of species A in species B
d_p	diameter of particle
g	acceleration due to gravity
g_u, g_l	statistical weights of atomic level u and level l
h	Planck's constant
I	transmitted light intensity
I_0	incident light intensity
k	Boltzmann's constant
k	thermal conductivity
κ	turbulent energy per unit mass of fluid
K	absorption coefficient
K_ν	spectral absorption coefficient
Kn	dimensionless Knudsen number
l	mixing length
L	absorption length in the medium
L_v	latent heat of evaporation
m	mass
M	molecular weight
N_l	atom population of level l
Nu	dimensionless Nusselt number
P_r	dimensionless Prandtl number
P_s	vapor pressure
R	inner radius of the plasma torch nozzle
R	universal gas constant
Re	dimensionless Reynolds number
Sc	dimensionless Schmidt number
Sh	dimensionless Sherwood number
t	time
T_{Fc}	temperature of the anode wall
T_g	temperature of the gas
T_m	maximum temperature of the plasma jet on torch axis at the nozzle exit
T_p	temperature of the particle
V_g	velocity of the gas
V_m	maximum velocity of the plasma jet on torch axis at the nozzle exit
V_p	velocity of the particle
y	distance from the jet centerline

Greek Symbols

$\Delta_{1/2}$	width of the line profile at mid-height
γ	ratio of heat capacity of gas at constant pressure to that at constant volume
ϵ	rate of dissipation of turbulent kinetic energy
λ	wavelength
ν	frequency of propagation
ρ	density
τ	particle relaxation time
ϖ	angular velocity

Subscripts

f	film
g	gas
p	particle

Table 1 Spraying Parameters Used to Study the Effect of the Gas Hydrogen Content on Powder Vaporization

Nozzle Diameter, mm	Total Gas Flow Rate Ar + H_2, slm	H_2 Content, %	Specific Enthalpy, MJ/kg
7	60	0-25	5.8

Table 2 Spraying Parameters Used to Study the Effect of Arc Current on Powder Vaporization

Nozzle Diameter, mm	Argon, slm	Hydrogen, slm	H_2 Content, %	Arc Current, A
7	45	15	25	300-600

It should be noted that the spraying conditions combining high arc current and hydrogen content may result in "overvaporization" of the metal powders, as compared to that observed under the industrial conditions generally used to spray iron-based powders.

2.2 Experimental Investigation of Powder Volatilization

2.2.1 Number Density of Metal Atoms in Jet Envelope. The species concentration was determined by means of absorption spectroscopy measurement of the light intensity, I, absorbed through a plasma of length (thickness) L. This technique allows the determination of the ground state population of atoms and ions, because the spectral lines rising from the ground state are absorbed proportionally to the number of absorbing elementary particles.

The incident, I_0, and transmitted, I, light intensities to the absorption coefficient K and the absorption length L in the medium are related as follows:

$$I = I_0 \, e^{-KL} \quad \text{(Eq 1)}$$

If the frequency, ν, of the incident light corresponds to a transition from the lower level (l) to the upper level (u) of atoms, the spectral absorption coefficient can be expressed as follows:[2]

$$K_\nu = [\lambda^2 \, g_u A_{ul} N_l \, (1 - \exp(-h\nu/kT)]/[8\pi g_l] \quad \text{(Eq 2)}$$

where A_{ul} is the transition probability from level u to level l, g_u and g_l are the statistical weights of levels u and l, λ is the wavelength corresponding to the ν frequency, T is the gas temperature, and N_l the population of level l. For the metal lines and temperature range of this study, the exponential term is less than 0.1 and can be neglected.

The absorption coefficient for a line of sight located at a distance y from the jet centerline was determined from the following expression:[3,4]

$$K(y) = \ln [I_0/I(y)] C_\nu \Delta_{1/2}(y) \quad \text{(Eq 3)}$$

where C_ν is a shape factor that takes into consideration the line

broadening by the Doppler and Lorentz effects, and $\Delta_{1/2}$ is the width of the light profile at mid-height.

The radial distribution of K in a jet cross section was established from the calculation of $K(y)$ and Abel's inversion procedure[2,4] assuming cylindrical symmetry. The absorption length L was inferred from the broadening of I at mid-height in various cross sections of the plasma jet.

The accuracy of the population density measurement depends on the accuracy of the estimation of the absorption length, the temperature value used in the calculation of line broadening, and the values of transition probabilities. It is estimated to be of the order of 15-20%. Figure 1 shows a schematic diagram of the experimental setup.[4,5]

The light of a hollow-cathode lamp was focused onto the plasma jet. The image of the measurement volume was formed at the entrance slit of a monochromator with a magnification of 3. The incident light of the lamp was modulated by using an optical chopper and the transmitted light was processed by means of a lock-in amplifier.

2.2.1 Size of Particles Originating from Vapor Condensation. Evaporated metal is either oxidized to the corresponding metal oxide or it condenses in the form of metallic fume. The resulting ultrafine particles were collected by means of a water-cooled probe connected to an electrical low-pressure impactor (DEKATI 95[6], Dekati, Ltd., Tampere, Finland). The latter enables real-time particle size distribution and concentration measurement. It is based on the combination of the electrical detection principle with low-pressure impactor size classification. The particles entrained in the sampling gas pass through a nozzle under the action of a soft vacuum; the heavier particles impact the plate and are retained, while the lighter particles are deflected and follow the streamlines to the next stage, and so forth.[7,8] The electric current carried by charged particles into each impactor stage is measured in real time by a sensitive multichannel electrometer.

The sampling tube was placed perpendicular to the plasma flow so that only the fine particles on the periphery of the jet were collected and not the sprayed particles within the jet cone (Fig. 2). Two diluters were placed between the sampling probe and the impactor. They ensured a 1/10 dilution of the sampled gas with pressurized air and avoided overloading of the sampling line. The impactor was composed of 12 stages and allowed the classification of particle sizes between 30 nm and 20 μm.

The probe "scanned" a distance between 10 and 100 mm downstream of the nozzle exit, in the axial direction, and between 11 and 20 mm in the radial direction.

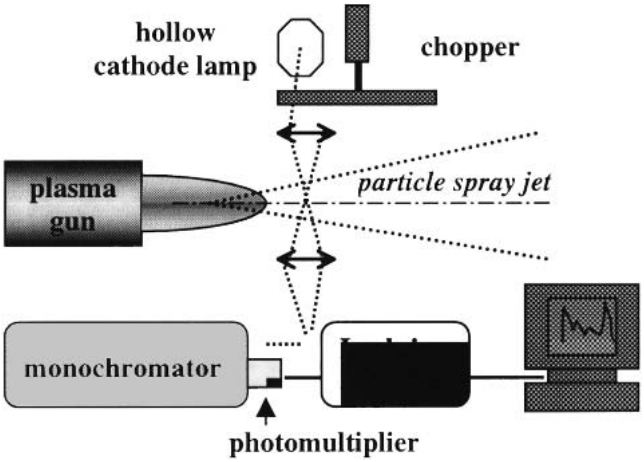

Fig. 1 Experimental set-up for absorption spectroscopy measurement

3. Modeling of Particle Vaporization

3.1 Mathematical Model of the Plasma Jet

The evaporation of metal particles in the plasma jet was studied using the commercial computational fluid dynamics (CFD) code FIDAP.[9] In the model, the argon-hydrogen plasma jet issued from a dc plasma torch into atmospheric air at constant pressure (10^5 Pa). The equations representing the mass, momentum, and energy balance were solved using a finite element method. The turbulent flow was modeled by the κ-ϵ model using the standard parameters.[10] The Boussinesq's eddy-viscosity model was used to predict the primary component of shear due to the entrained air.

The gas flow model was based on the following assumptions: (1) the system was steady and in local thermodynamic equilibrium (LTE), (2) the plasma was optically thin, and (3) no chemical reaction or demixing occurred in the gas phase.

The computational domain is shown in Fig. 3. The simulations were performed in 2D coordinates with a nonuniform grid. The mesh density was higher near the torch exit and in the core of the plasma jet, where the highest gradients were supposed to be located. The length of the calculation domain was 105 mm and its radius 21 mm, which is six times the nozzle radius. At the inlet of the domain, i.e., the gun exit, the values of the different

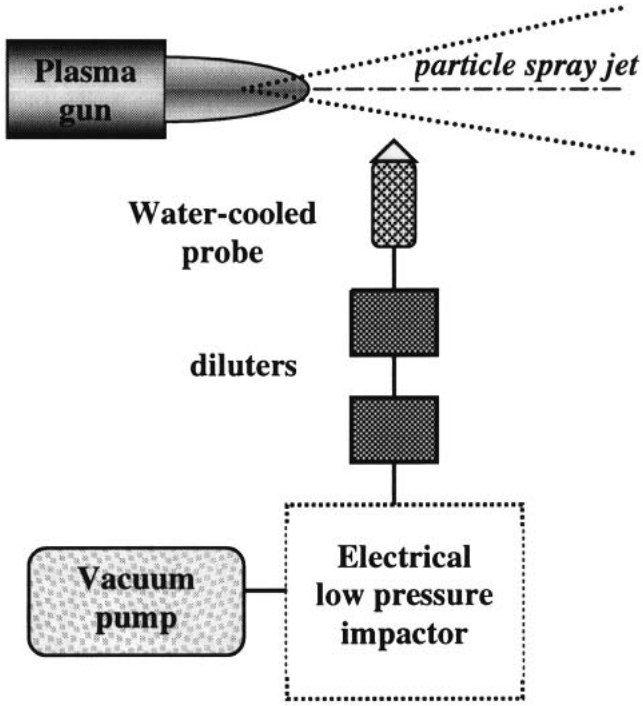

Fig. 2 Schematic diagram of the system used to collect the micronic particles

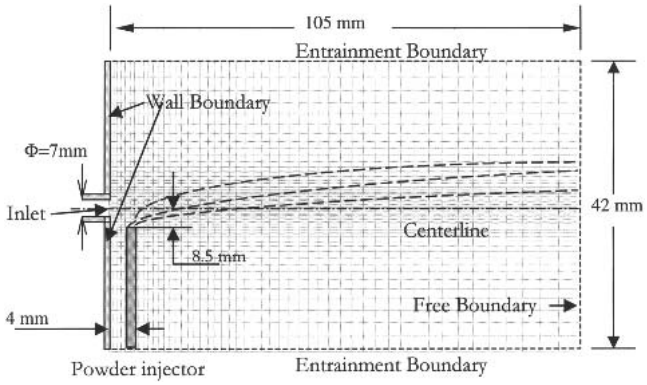

Fig. 3 Calculation domain

variables were fixed and the following radial profiles were used for the temperature and the axial component of the velocity:[11]

$$T_g(r) = (T_m - T_c)\left(1 - \left(\frac{r}{R}\right)^{4.5}\right) + T_{Fc} \quad \text{(Eq 4)}$$

$$V_g(r) = V_m\left(1 - \left(\frac{r}{R}\right)^{2}\right) \quad \text{(Eq 5)}$$

where T_m and V_m are the temperature and velocity of the plasma jet at the torch axis, and T_{Fc} is the temperature of the anode, set to 550 K. T_m and V_m were computed from the enthalpy balance and mass flow rate at the nozzle exit, with respect to process parameters.

The turbulence boundary conditions involved the calculation of κ and ϵ at the torch exit. These calculations consisted of estimating the inflow profile of $\kappa(r)$, using the gas velocity profile at the torch exit $V_g(r)$ and turbulence intensity I set to 0.005. The dissipation rate profile $\epsilon(r)$ was then deduced from the profile of $\kappa(r)$ and a mixing length model was applied to the interior of the nozzle. The turbulent kinetic energy and its dissipation rate at the inlet were specified by:[9]

$$\kappa(r) = 0.0005 V_g^2(r) \quad \text{(Eq 6)}$$

$$\varepsilon(r) = k(r)^{3/2}/l \quad \text{(Eq 7)}$$

The mixing length was calculated from $l = 0.075\delta/C_\mu^{3/4}$, where C_μ is the turbulent constant and δ is the radial distance at which the gas velocity is equal to 1/10 of the maximum inflow velocity, i.e.,

$$V_{g,\delta/2} = 0.1\ V_{g,max} \quad \text{(Eq 8)}$$

The exit plane of the domain had an initial fixed temperature at 550 K. The other boundaries were free, that is, the only condition applying to them was an imposed pressure, set equal to atmospheric pressure; the flow at these open boundaries was calculated and could be either inward or outward depending on the location. The gas flow was assumed to be made up of two gases: the plasma-forming gas and the ambient gas. The thermodynamic and transport properties of the gas mixture were calculated using the laws of mixtures and the data of pure gases. The latter were obtained from Boulos et al.[12]

3.2 Heat Transfer and Vaporization of Metal Particles

Models of the in-flight behavior of particles in plasma spraying usually take into account the steep variations of the fluid temperature in the boundary layer surrounding particles, the Knudsen effect, plasma-particle interactions, heat transfer within the particle, vaporization of the particle material, and other factors. However, these calculations often neglect the effect of the evaporation on the particle motion and heating. This is a reasonable assumption when the mass loss due to evaporation is fractionally small. However, under certain conditions, the particle mass loss by evaporation and the vapor cloud around the particles affect the dynamics characteristics appreciably.

In the present study, the effects of plasma-particle interactions and particle mass loss were incorporated in the model of particle heating and acceleration by means of simple analytical forms. The Lagrangian technique was used to couple the fluid dynamics of the gas flow to that of the particles.

The following assumptions were made in the analysis of plasma-particle interactions: (1) particles were spherical, (2) there was no temperature gradient within the particles, (3) the forces of gravity, thermophoresis, Basset history, and the effect of particle electric charging[13] were negligible, (4) local thermodynamic equilibrium existed in the boundary layer surrounding particles, and (5), the particle turbulent dispersion was taken into account.

The most important factor for the motion of a powder particle in a plasma jet is the viscous drag force. Other forces, such as those due to pressure gradient, the Basset force, the thermophoretic force, etc., are very small in comparison. On the basis of the above considerations, the equation of motion of a powder particle was expressed as follows:[9]

$$\frac{dV_p}{dt} = \frac{(V_g - V_p)}{\tau} + \frac{(\rho_p - \rho_g)}{\rho_p} g - \varpi \times (\varpi \times r) - 2\varpi \times V_p \quad \text{(Eq 9)}$$

where ϖ is the angular velocity and τ is the particle relaxation time defined by

$$\tau = \frac{4\rho_p d_p}{3\mu_g C_D \mathrm{Re}} \quad \text{(Eq 10)}$$

The temperature of the particle along its trajectory was deduced from a heat balance in the boundary layer surrounding the particle. The heat transferred to the particle by conduction and convection form the plasma gas is equal to the increase of sensible heat plus the latent heat of evaporation L_v:

$$h\pi d_p^2 (T_g - T_p) = m_p C_{p,p} \frac{dT_p}{dt} + L_v \frac{dm_p}{dt} \quad \text{(Eq 11)}$$

where h is the plasma-particle heat transfer coefficient.

The rate of mass loss from the particle is equal to the mass transfer of vapor by convection away from the surface

$$\frac{dm_p}{dt} = k_d \rho_g \pi d_p^2 (c_{Fe,g} - c_{Fe,p}) \quad \text{(Eq 12)}$$

where k_d is the mass transfer coefficient, $c_{Fe,g}$ is the concentration of metal in the bulk fluid, and $c_{Fe,p}$ is the concentration of metal at the surface of the particle. The latter is defined as

$$c_{Fe,p} = \frac{p_s M}{\rho_g R T} \quad \text{(Eq 13)}$$

where M is the molecular weight of metal, R is the universal gas constant, ρ_g and T are the density and temperature of the fluid at the particle wall temperature, respectively, and p_s is the corresponding saturation vapor pressure as determined from the Clausius-Clapeyron relationship:

$$p_s = p_{ref} \exp\left[-\frac{L_v M}{R T_{ref}} \left(\frac{T_{ref}}{T} - 1 \right) \right] \quad \text{(Eq 14)}$$

where p_{ref} and T_{ref} are a pair of values corresponding to one point on the Clausius-Clapeyron curve.

The following equation was used for the drag coefficient C_D:[14]

$$C_D = 23.707 Re^{-1} (1 + 0.165 Re^{2/3} - 0.5 Re^{-0.1}) f_1 f_2 \quad \text{(Eq 15)}$$

This equation is valid for Reynolds number ranging between 0.15 and 500. The particle Reynolds number is defined by

$$Re = \frac{d_p |V_p - V_g| \rho_g}{\mu_g} \quad \text{(Eq 16)}$$

The correction fractors f_1 and f_2 account for the temperature gradient within the particle boundary layer and the Knudsen effect, respectively. These factors were expressed by the following equations:[13-15]

$$f_1 = \left[1 + \left(\frac{2 - a}{a} \right) \left(\frac{\gamma}{1 + \gamma} \right) \left(\frac{4}{Pr_p} \right) Kn \right]^{-0.45} \quad \text{(Eq 17)}$$

$$f_2 = \left(\frac{\rho_p \mu_g}{\rho_g \mu_p} \right)^{0.15} \quad \text{(Eq 18)}$$

where a is the thermal accommodation coefficient, γ is the specific heat ratio, Pr_p is the Prandtl number at the surface temperature of the particle, Kn is the Knudsen number, which was assumed to be constant at 0.1.[20]

Considering the effect of mass loss along the trajectory, the drag coefficient C_D is modified to $C_{DV} = C_D/(1 + B)$[16] where B is the Spalding number,

$$B = \frac{C_{vap}(T_g - T_p)}{K_v} \quad \text{(Eq 19)}$$

where C_{vap} is the specific heat of metal vapor, and L_v is the latent heat of vaporization.

The Nusselt number was expressed by the modified Ranz-Marshall equation:

$$Nu = f_3 f_2 (2 + 0.6 Re^{0.5} Pr^{1/3}) / (1 + B_m) \quad \text{(Eq 20)}$$

where

$$f_3 = \left[1 + \left(\frac{2 - a}{a} \right) \left(\frac{\gamma}{1 + \gamma} \right) \left(\frac{4}{Pr_p} \right) Kn \right]^{-1} \quad \text{(Eq 21)}$$

The Spalding number for mass transfer B_m is equal to $(c_s - c_g)/(c - c_s)$.[16] In the present case, the concentration in the particle c is equal to 1; c_g and c_s are the concentrations in the plasma gas and at the particle surface, respectively. The Sherwood number is expressed by the following form:

$$Sh = (2 + 0.6 Re^{0.5} Sc^{1/3}) / (1 + B_m) \quad \text{(Eq 22)}$$

In the simulation of the acceleration and heating of the sprayed particles, the thermophysical properties of iron were obtained from Ref. 17.

4. Results and Discussion

4.1 Iron Atom Concentration in Various Cross Sections of the Plasma Jet

Spectroscopic measurements were performed at a distance from 60-120 mm from the nozzle exit. At less than 60 mm, the plasma emission light is higher than that emitted by the metal vapor and measurements would require a higher-power light source than that used in this study.

Figure 4 shows the results of measurements for the 14-55 μm iron powder injected in the plasma jet at a feed rate of 200 g/h. The iron atom concentration is of the order of 3×10^{21} atoms/m^3 on the jet axis at 60 mm, and decreases further downstream. Indeed, the decrease in plasma flow temperature results in a lessening of particle evaporation but also favors the condensation of vapor to submicronic particles. The temperature of the

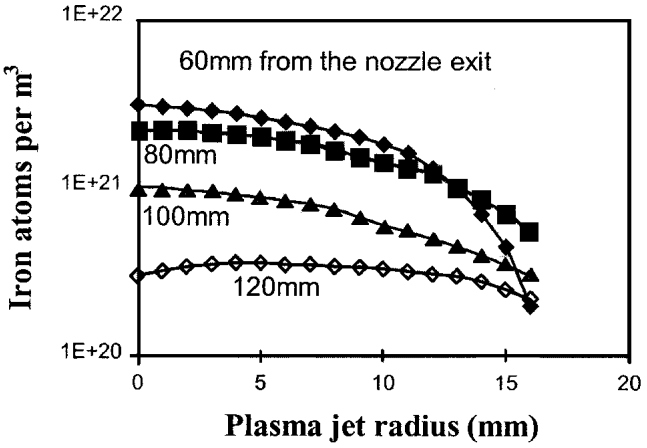

Fig. 4 Iron atom concentration in different cross sections of the plasma jet. Particle size range: 14-55 μm; powder feed rate: 200 g/h

gas flow is about 6500 K at the jet centerline at 60 mm, and 3000 K at 120 mm. At the latter distance, the detected atoms originate mostly from the vapor formed upstream and entrained with the flow. In addition, the condensation of vapor to submicronic particles lowers the vapor pressure and facilitates further evaporation downstream.

Experiments carried out with powder feed rates ranging from 50-500 g/h showed that the iron vapor concentration in the flow was proportional to the powder feed rate.

4.2 Effect of the Hydrogen Content of the Plasma-Forming Gas

Hydrogen is often used in plasma spraying as a secondary gas to improve the melting of particles because of its high conductivity (5.4 W/m · K at 12,000 K) as compared to that of argon (1.5 W/m · K at 12,000 K). Moreover, the arc voltage and the enthalpy input to the gas are increased by a factor 1.4 to 2 by adding a small fraction of hydrogen. The effect of hydrogen concentration in the plasma gas on the degree of vaporization is illustrated in Fig. 5.

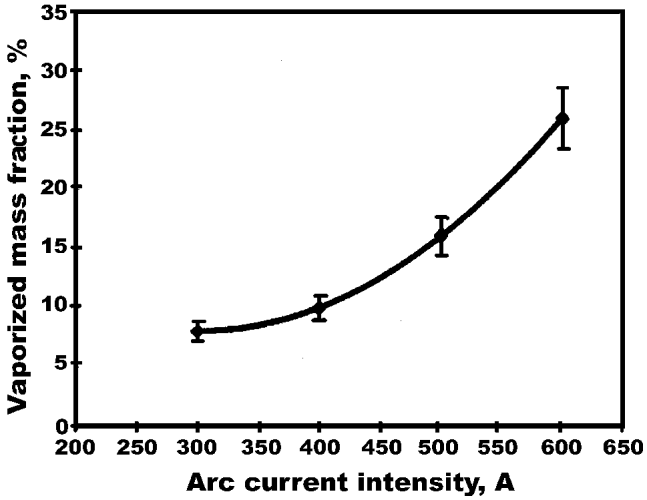

Fig. 5 Effect of the hydrogen content of the plasma-forming gas on the vaporized mass fraction. Particle size range: 14-55 μm. Powder feed rate: 500 g/h

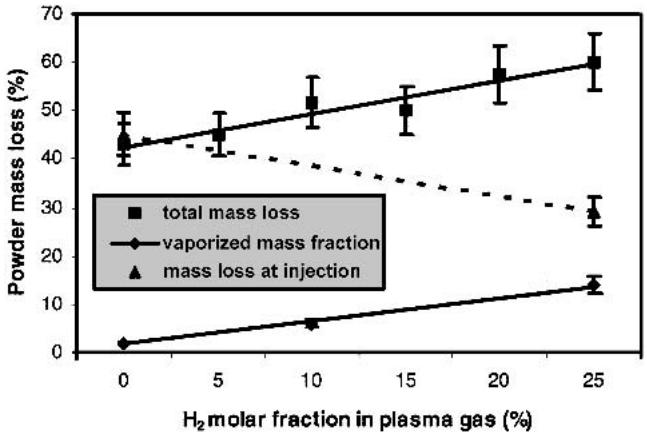

Fig. 6 Variation of the powder mass loss with the hydrogen content of the plasma forming. Particle size range: 14-55 μm; powder feed rate: 500 g/h

The vaporized mass fraction increased from 2-14% when the hydrogen content was raised from 0-25% (spraying conditions of Table 1). The fraction of powder lost at the injection point was taken into account to determine the quantity of powder occluded in the plasma jet. The powder fraction that did not penetrate the jet was estimated from a 2D laser imaging technique.[4] This technique makes it possible to determine the amount of "hot" and "cold" particles in the flow from the thermal radiation emitted by particles and the light scattered by particles passing through a laser sheet.

This study was conducted with metal powders, but similar experimental observations have been made with low-conductivity and high-melting temperature particles such as ceramic powders. In that case, the heat flux transferred from the plasma is high relative to the amount of energy that particles can absorb. This induces a rapid increase in particle surface temperature and, consequently, in vaporization rate.

The overall deposition efficiency, in plasma spraying, depends on powder injection efficiency, degree of particle vaporization, and molten state of particles at impact with the substrate. In this study, the observed loss of powder by vaporization was always lower than the loss at the injection point (Fig. 6). The powder mass loss at the entry of the feed in the jet varied between 45% and 30%, as the hydrogen content of the plasma gas was increased from 0-25%. As the argon flow rate and the arc current were decreased, in order to compensate for the arc voltage increase from the higher fraction of hydrogen, the momentum of the constant mass flow at the nozzle exit diminished. Therefore, it was easier for finer particles to penetrate the jet.

4.3 Effect of Arc Current

The arc current was increased from 300-600 A at a total gas flow rate of 60 slm and H_2 concentration of 25%. This resulted in an increase in gas specific enthalpy and increased the vaporized mass fraction from 8% to 25% (Fig. 7).

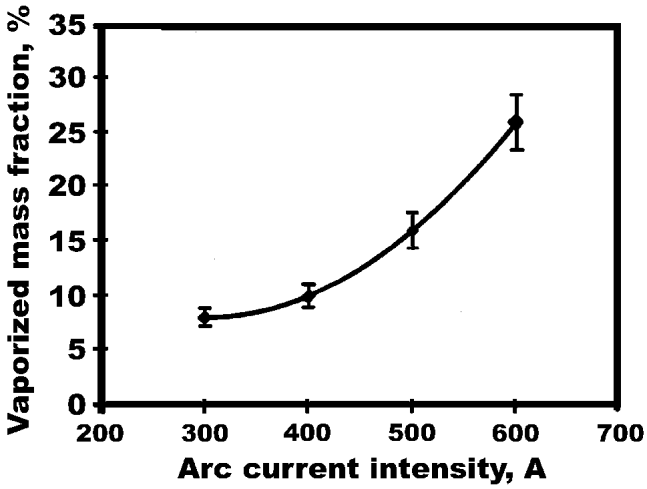

Fig. 7 Effect of arc current on the vaporized mass fraction. Particle size range: 14-55 μm. Powder feed rate: 200 g/h

4.4 Effect of Particle Size

Figure 8 shows the radial distribution of vapor concentration at an axial distance of 100 mm from the nozzle exit. As expected, evaporation was higher for the finer-size particle powder. The predictions of the model show that particles of diameters higher than 90 μm do not undergo any evaporation (Fig. 9). Therefore, the vapor detected in the spraying of the 80-100 μm and 125-160 μm powders must be due to the small fraction of finer particles in these powders.

For the spraying conditions of Table 1 (600 A and 25% volume of hydrogen), the computed fraction of vaporized mass was about 23% for the 14-55 μm powder (Fig. 10). This result was in good agreement with the experimental results for the same particle size and operating conditions. They showed a vaporized mass fraction of about 25% (Fig. 9). However, it should be noted that the experimental vaporized mass is related to the powder that has actually penetrated in the jet flow, whereas the computation is based on the total amount of powder fed in the jet.

When the powder loss at the injection (about 30% for the spraying conditions of the study) is taken into account, a calculated vaporized mass fraction of about 20% results.

4.5 Collection of Submicronic Particles

Figure 11 shows the increase in concentration of submicronic particles, collected using the impactor device, with distance from the plasma nozzle. Measurements were performed at axial distances between 20 and 110 mm from the nozzle exit and 15 mm off the jet centerline.

The concentration of submicronic particles ranges from 2.5×10^8 at 20 mm to 5×10^9 at 110 mm and exhibits a rapid increase at 40 mm. This corresponds to the end of particle vaporization, except for the finest particles (Fig. 9). In addition, the mixing of the plasma jet with the surrounding air results in a rapid decrease in flow temperature and, therefore, in an increase in vapor condensation.

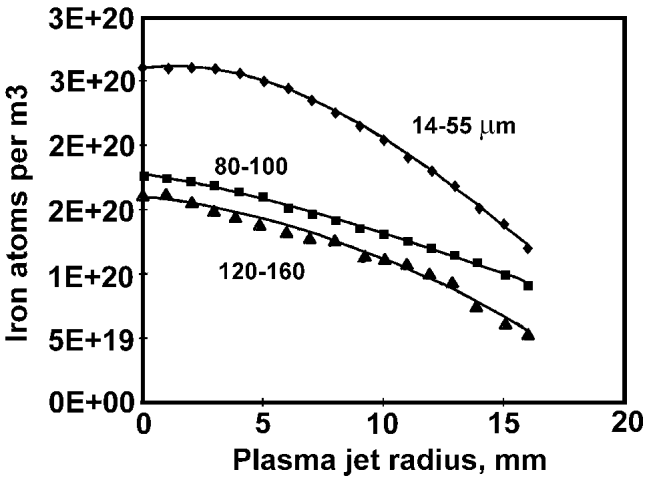

Fig. 8 Iron atom concentration at 100 mm from the nozzle exit for various particle size ranges. Powder feed rate: 50 g/h

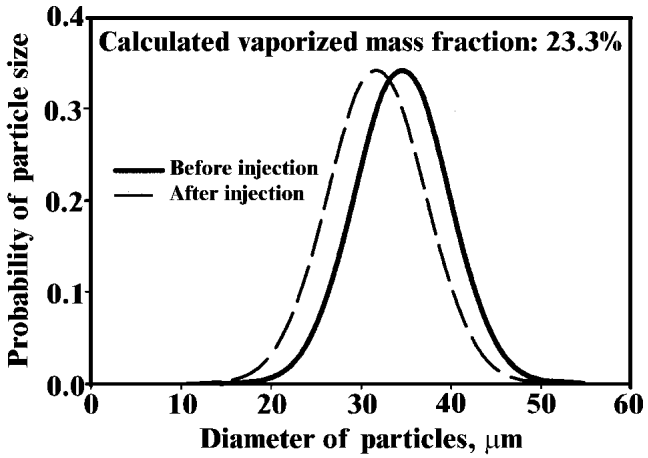

Fig. 10 Computed distribution of vaporized mass fraction for various particle size ranges

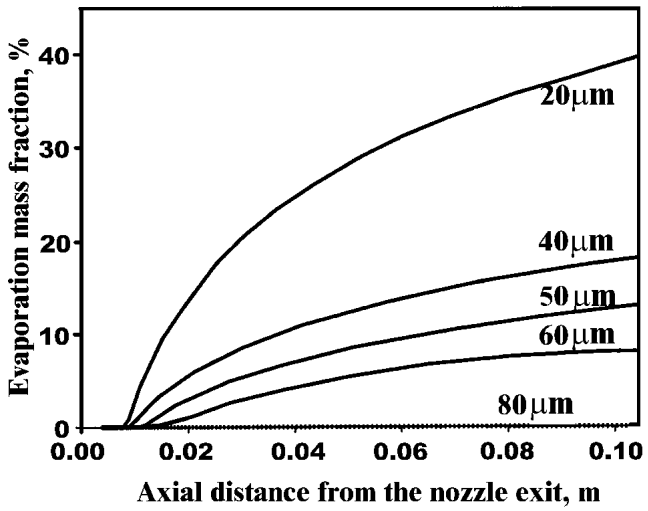

Fig. 9 Evolution of particle vaporized mass fraction with distance to nozzle exit

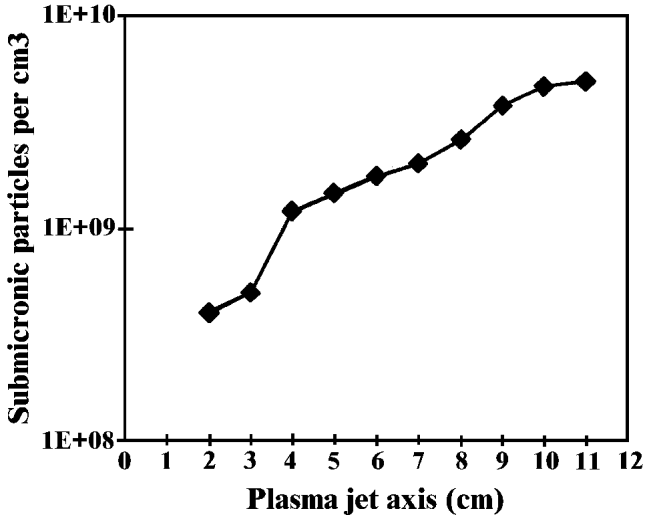

Fig. 11 Iron submicronic particle concentration at a radial distance of 15 mm from the jet centerline

The size distribution of the fume at 50 mm is shown in Fig. 12. Most of the particles have a diameter less than 0.05 μm. Further downstream, the concentration of larger diameter particles increases as the gas flow cools.

If we assume that the average submicronic particle diameter is 0.05 μm, the particulate content in the atmosphere is in the order of 40 mg/m^3 close to the plasma jet. This value decreases to an average value ranging between 0.1 and 8 mg/m^3 in the spray booth, corresponding to a particle concentration between 10^5 and 10^7/cm^3 (Fig. 13). Figure 13 indicates that there is a relationship between mass concentration and particulate number concentration for iron particles of diameters ranging between 0.025 and 0.5 μm; it also shows the maximum allowable limits (24-h average) set by the National Ambient Air Quality Standards (NAAQS) of U.S. Environmental Protection Agency (EPA)[1] for particulates of diameter less than 2.5 μm (PM-2.5)

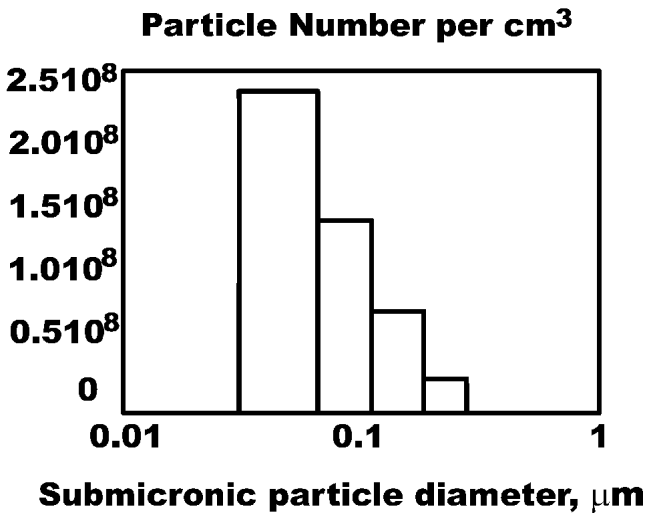

Fig. 12 Iron submicronic particle concentration at an axial distance of 50 mm and a radial distance of 15 mm from the jet center line

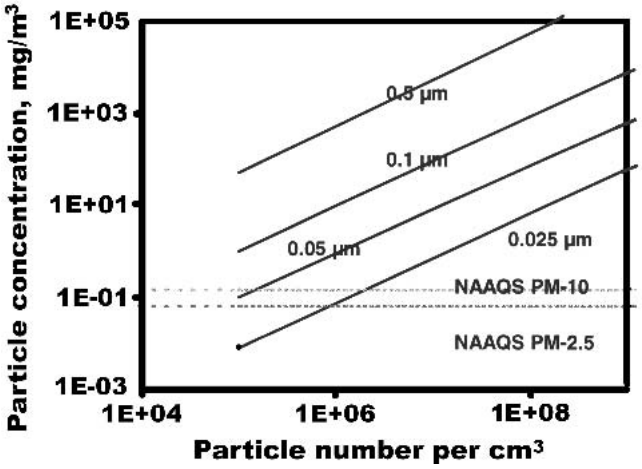

Fig. 13 Particulate mass concentration versus particulate number concentration for iron particles. NAAQS: National Ambient Air Quality Standards. PM-2.5: particle concentration of diameter less than 2.5 μm; PM-10: particle concentration of diameter less than 10 μm.

and 10 μm (PM-10). They are 0.065 mg/m and 0.150 mg/m^3, respectively.

Similar experiments were conducted to analyze the atmosphere of the spray booth during the spraying of NiCrAlY with a high-power PlazJet plasma gun and a twin-wire arc spray system operated under industrial conditions.[18] They showed that the dust concentration, at a height of 1 m from the floor, was in the order of 75 mg/m^3 for plasma spraying and ranged between 100 and 130 mg/m^3 for arc spraying. The latter is generally associated with a high degree of vaporization of the sprayed droplets, because the tips of the wires are overheated by the arc prior to gas atomization. For both spraying systems, the size of the collected submicronic particles was less than 0.4 μm.

The particulate emission in the spray booths is usually higher than the EPA limits. However, because the exhaust gas generally undergoes a cleaning operation, either by means of bag filter or wet scrubbing, the gas emission from thermal spray processes meet the air quality standards. Nevertheless, the larger particles that fall on the booth floor because they do not penetrate the jet or do not stick on the part must be carefully recovered, especially when working with hazardous materials as chromium, nickel, copper, cobalt, aluminum, and zinc.[1,19]

5. Conclusions

An experimental study of iron powder vaporization in the plasma-spraying of iron powders was carried out using (1) absorption spectroscopy to determine the concentration of metal atoms in the flow and (2) collection and analysis of the dust formed by the condensation of vapor to submicronic particles, to evaluate the mass concentration and size distribution of these particles in the atmosphere of the spray booth.

The degree of vaporization and size evolution of the droplets were also derived from the simulation of the plasma jet and plasma particle interactions with the CFD code FIDAP. There was good agreement between computed and experimentally observed degrees of vaporization of iron particles.

The experimental observations showed that, under the conditions of the study, the dust concentration in the atmosphere of the plasma spray booth ranged between 40 and 0.1 mg/m^3, and that particle sizes in the collected fume samples were less than 0.5 μm. Similar observations during the spraying of NiCrAlY alloy with a PlazJet plasma gun and a twin-wire arc spray system resulted in a dust concentration of 75 mg/m^3 for the plasma system and between 100 and 130 mg/m^3 for the arc spray device. In both cases, the dust particle diameter was less than 0.4 μm. The degree of vaporization of powders was found to depend on the specific enthalpy and thermal conductivity of the plasma gas.

It was also found that, under the conditions of this study, most of the powder loss occurred at the injection point. This effect was more pronounced for the finest particles (<15 μm) because of their lower momentum at the injector exit.

Acknowledgments

The authors thank Christian Trassy and K.-I. Li for their help with the experiments on particle vaporization. This work was supported by CNRS-France under the ARC-grant for the study of plasmas reactors and by the Earth Engineering Center of Columbia University for the modeling study.

References

1. U.S. Environmental Protection Agency: "Report on Waste Minimization in Metal Finishing Industries," EPA, Washington, DC, 1996, 530-R-96-008.
2. H.R. Griem: *Plasma Spectroscopy,* McGraw Hill, New York, 1964.
3. M. Mitchell and M. Zemansky: *Resonance Radiation,* Cambridge University Press, London, 1971.
4. K.-I. Li: "Contribution to the Study of Particle Injection and Vaporization in d.c. Plasma Spray Jets," Ph.D. Thesis, University of Limoges, France, Laboratory SPCTS, March 1998.
5. K.-I. Li, M. Vardelle, A. Vardelle, P. Fauchais, and C. Trassy: "Vaporization of Metal Powders in Plasma Sprays" in *Practical Solutions for Engineering Problems,* C.C. Berndt, ed., ASM International, Materials Park, OH, 1996, pp 547-52.
6. DEKATI Measurements Oy, Tampere, Finland (www.dekati.fi).
7. J. Keskinen, K. Pietarinen, and M. Lehtimaki: "Electrical Low Pressure Impactor," *J. Aerosol Sci., 23,* 1992, pp. 353-60.
8. K.A. Gross, P. Fauchais, M. Vardelle, J. Tikkanen, and J. Keskinen: "Vaporization and Ultra-Fine Particle Generation during the Plasma Spraying Process" in *A United Forum for Scientific and Technological Advances,* C.C. Berndt, ed., ASM International, Materials Park, OH, 1997, pp. 543-48.
9. FIDAP 7.62 Code, Fluid Dynamics International, Inc., Lebanon, NH, 1997.
10. N.J. Themelis: *Transport and Chemical Rate Phenomena,* Gordon Breach, New York, 1995, pp. 67-72.
11. J.D. Ramshaw and C.H. Chang: "Component Fluid Dynamics Modeling of Multicomponent Thermal Plasma," *Plasma Chem. Plasma Process., 1992, 12*(3), pp. 299-325.
12. M.I. Boulos, P. Fauchais, and E. Pfender: *Thermal Plasma: Fundamentals and Applications,* Vol. 1, Plenum Press, New York, 1994.
13. E. Pfender and Y.C. Lee: "Particle Dynamics and Particle Heat and Mass Transfer in Thermal Plasma. Part I. The Motion of a Single Particle without Thermal Effects," *Plasma Chem. Plasma Process.* 1985, *5*(3), pp. 211–37.
14. B. Dussoubs, "3-D Modeling of Plasma Spray Process: Influence of Injection Conditions of Powders and Spraying Parameters on Particle Acceleration, Heating and Distribution in the Flow," Ph.D. Thesis, University of Limoges, France, 1998 (in French).
15. P. Nylen, "The Prediction of Fluid Flow, Particle In-flight and Coating Characteristics in Atmospheric Plasma Spraying," Ph.D Thesis, Chalmers University of Technology, Göteborg, Sweden, 1999.
16. A. Berlemont, M.S. Gramcher, and G. Gouesbet: "On the Lagrangian Simulation of Turbulence Influence of Droplet Evaporation," *Int. J. Heat Mass Transfer,* 1991, *34,* pp. 2805-12.
17. E.A. Brandes, *Smithells Metals Reference Book,* 6th ed., Butterworths, London, 1983.
18. D. Sacriste, N. Goubot, J. Dhers, M. Ducos, and A. Vardelle: "An Evaluation of the Electric Arc Spray and HPPS Processes for the Manufacturing of MCrAlY Coatings," *J. Thermal Spray Technol. 10,* 2001, pp. 352-58.
19. I.K. Wernick and N.J. Themelis: "Recycling Metals for the Environment," *Annu. Rev. Energy Environ.,* 1998, *23,* pp. 465-97.
20. V.V. Sobolev, J.M. Guilemany, and A.J. Martin, "In Flight Behavior of Steel Particles during Plasma Spraying," *J. Mater. Process. Technol.* 1999, *87,* pp. 37-45.